Journal of Physical Science, Vol. 34(2), 41–57, 2023

Irradiation-Assisted Hydrothermal Conversion of Water Hyacinth Leaves to Fluorescence Carbon Dots with High Quantum Yield

Tanagorn Kwamman,[1] Threeraphat Chutimasakul,[1] Panida Sangangam,[2] Nattamon Puengposop,[2] Pattanapong Thangsunan,[3] Tinutda Phonlam[4] and Kanokorn Wechakorn[2*]

[1] Nuclear Technology Research and Development Center, Thailand Institute of Nuclear Technology (Public Organisation), Nakorn Nayok 26120, Thailand
[2] Department of Chemistry, Faculty of Science and Technology, Rajamangala University of Technology Thanyaburi, Pathum Thani 12110, Thailand
[3] Division of Biochemistry and Biochemical Innovation, Department of Chemistry, Faculty of Science, Chiang Mai University, Chiang Mai 50200, Thailand
[4] Department of Materials and Metallurgical Engineering, Rajamangala University of Technology Thanyaburi, Pathum Thani 12110, Thailand

[*]Corresponding author: kanokorn_w@rmutt.ac.th

Published online: 25 August 2023

To cite this article: Kwamman, T. et al. (2023). Irradiation-assisted hydrothermal conversion of water hyacinth leaves to fluorescence carbon dots with high quantum yield. *J. Phys. Sci.*, 34(2), 41–57. https://doi.org/10.21315/jps2023.34.2.4

To link to this article: https://doi.org/10.21315/jps2023.34.2.4

ABSTRACT: *Electron beam irradiation (EBI) (100−400 kGy) was utilised to pretreat water hyacinth (WH). Scanning electron microscopy (SEM), X-ray photoelectron spectroscopy (XPS), fourier transform infrared (FTIR), UV-vis absorption and fluorescence spectroscopy were used to examine the effects of EBI and hydrothermal temperatures on the physical, chemical and optical characteristics of carbon dots (CDs). The combination of 400 kGy-pretreatment and 250°C-hydrothermal treatment as the optimal condition for CDs synthesis provided the highest quantum yield (QY) of 14.5% and the product yield of 7.5%. Using dynamic light scattering (DLS), the CDs showed an average size of around 180 nm, and the zeta potential analysis revealed the overall negative charge on the CDs' surface. In comparison, the CDs synthesised via hydrothermal conversion at 250°C without EBI showed a QY of only 4.0% and a product yield of 3.8%, significantly lower than the condition with 400 kGy-pretreatment. The improved optical characteristics of the CDs could result from the high nitrogen contents of WH biomass, oxygen-rich surfaces from EBI pretreatment at 400 kGy and the aromatic skeleton of the CDs.*

Keywords: carbon dot, irradiation processing, electron beam, hydrothermal, water hyacinth

1. INTRODUCTION

Water hyacinth (WH) (*Eichornia crassipes*) grows rapidly, leading to obstruction of water flow and insufficient oxygen dissolution in rivers and canals.[1–4] However, WH contains rich natural carbon sources, including cellulose (~30%), hemicellulose (~29%), lignin (19%) and protein, up to 22%.[1–4] Lignocellulose biomass (LCB) is composed primarily of lignin, cellulose and hemicellulose, with trace amounts of acetyl groups and minerals. Moreover, WH contains natural nitrogen and other elements, depending on its origin. It has a rigid structure due to extensive intramolecular and intermolecular hydrogen bonding.[5] The complex network of hemicellulose, lignin and cellulose provides a rigid-plant cell wall by linking cellulose fibers into microfibrils and cross-linking with lignin, and the complexity of the network also depends on plant species, tissues and maturity.[6] LCB can be refined into valuable resources, such as biofuel, chemicals, polymers, biochar, activated carbon and carbon dots (CDs). However, the natural complex and rigid lignocellulose structure, which includes high cellulose crystallinity, cellulose degree of polymerisation and lignin contents, can make the deconstruction processes cumbersome.[7] Therefore, the pretreatment of LCB is needed to disrupt the recalcitrant structure for hydrolysis processes.

In general, several pretreatment methods, such as mechanical, chemical, physicochemical and biological methods, are employed to improve accessibility and biodegradability for enzymatic or chemical actions.[7] For the mechanical method, Yoo et al. subjected the soybean hulls to extrusion pretreatment for an enhanced generation of fermentable sugars with a high glucose yield of 95% with screw speed, barrel temperature and in-barrel moisture content of 350 rpm, 80°C and 40%, respectively.[8] Moreover, acid-based pretreatments, including hydrochloric acid (HCl) and sulfuric acid (H_2SO_4), were used for hemicellulose dissolution. For example, Liu et al. demonstrated a two-stage process, which was the diluted acid pretreatment (0.7 wt% diluted HCl, 120°C for 40 min) followed by the wet milling (for 15 min) of corn stover. This resulted in high sugar recovery (81% xylose, 64% glucose) even at a very low cellulase enzyme dosage of 3 FPU/g of the substrate.[9] However, the main disadvantage of acid-based pretreatments is corrosive, necessitating the use of costly non-metallic reactors and raising the overall cost. In addition, process complexity is due to acid toxicity, the need for neutralisation and wastewater treatment. Alkaline-based pretreatments can also be used for disrupting the lignin structure and breaking the bonds (ester, aryl-ether, C-C bond) associated with lignin and carbohydrate polymers.[7] However, the alkaline-based pretreatments using sodium hydroxide (NaOH), potassium hydroxide (KOH), calcium hydroxide [$Ca(OH)_2$] and ammonium hydroxide (NH_4OH) can cause cellulose swelling and debonding between lignin

and cellulose. Thermal-assisted mild NaOH 2% (w/w) treatment of rice husk showed highly efficient lignin removal of 54% (w/w) and increased cellulose concentration as high as 51.65% (w/w).[10] Oxidative treatments such as hydrogen peroxide can detach lignin from lignocellulose biomass. The combination of H_2O_2 and alkali [NaOH and sodium hypochlorite (NaClO)] improved the ethanol yield of Barley straw by 79.3%–84.6%.[11] However, anaerobic digestion can be inhibited by hydrogen peroxide (H_2O_2) concentrations above 4%.[11] These pretreatment methods required toxic chemicals, organic solvents or high temperatures.

The radiation process is an alternative green technique for the pretreatment method. Both gamma and electron beam irradiation can produce free radicals, which could degrade polysaccharide chains and cell wall deconstruction via glycosidic bond scission.[12,13] The major advantage of electron beam irradiation (EBI) and gamma pretreatments is a clean, efficient and cost-effective techniques because there is no demand for temperature or pressure adjustments with the additional requirement of chemicals/solvents.[7] From the previous studies, gamma irradiation at a high dose (500 kGy) reduced biomass particle size and glucose yield.[12,14] EBI at 0.5 kGy–50 kGy resulted in significant cellulose degradation.[7]

LCB is a promising carbon source for the synthesis of CDs.[15–20] CDs stand out as a new material that combines the exceptional properties of graphene and CDs, such as excellent electrical conductivity, enlarged surface area, high solubility in a range of solvents, strong luminescence, high mobility, decreased chemical impedance and tunable bandgap.[15–19] CDs can be classified into graphene quantum dots (GQDs), carbon nanodots (CNDs) and polymer dots (PDs). CDs are promising for their applications in fluorescence sensors, bioimaging, photovoltaic devices, light-emitting diodes, solar cells, fuel cells, batteries and supercapacitors.[15–19,21,22] The synthesis of CDs can be conducted from LCB via several techniques, such as hydrothermal, electrochemical, microwave, electron beam lithography or thermal treatments.[23] Through molecular oxidation with strong acids [H_2SO_4 and nitric acid (HNO_3)], Yang et al. reported the large-scale production of GQD [6% quantum yield (QY)] from Chinese ink with a high product yield (80%).[24] Suryawanshi et al. synthesised GQDs (1% QY) by refluxing the turbostratic carbon mixed with H_2SO_4 and HNO_3 at 90°C for 5 h.[25] The hydrothermal method is another technique for GQDs fabrication. Pan et al. cut the graphene sheet into GQDs (6.9% QY) via hydrothermal treatment at 200°C for 10 h (5% product yield).[26] Atchudan et al. synthesised nitrogen-doped CDs from *Chionanthus retusus* fruit extract using a simple hydrothermal-carbonisation method.[27] Nitrogen passivation can enhance the fluorescence emission of the CDs by inducing an upward shift in the fermi level and electrons in the conduction band.[28,29] Nitrogen-doped CDs from *Poa Pratensis* were prepared by a one-step hydrothermal treatment with a QY of 7%.[30] They also developed nitrogen-doped CDs from *Phyllanthus acidus* fruit juice by the

hydrothermal method in aqueous ammonia with a QY of 14%.[31] The hydrophilic nitrogen-doped CDs were prepared from the dwarf banana peel by a hydrothermal method with a good QY (23%) for multicolor bioimaging and fluorescent ink.[32] Nitrogen-doped GQDs from Neem leaf extracts were synthesised by combining pyrolysis and hydrothermal treatment with a 25% production yield and 46% QY.[33]

In this study, facile and green electron beam irradiation (EBI)-assisted hydrothermal conversion was used to synthesise the CDs from WH. The WH is suitable for CDs production in terms of its high natural carbon and nitrogen contents as well as being environmental friendliness. The effects of EBI dose and hydrothermal temperatures on the physiochemical and optical properties of CDs were investigated. Our synthesis approaches are practical and can provide high product yield and QY with the aim of less toxic chemicals and waste compared to the previous reports. Additionally, the potential for large production of the CDs can be achieved by combining hydrothermal and irradiation processes.

2. EXPERIMENTAL AND METHODS

2.1 Materials and Instrumentation

Quinine hemisulfate monohydrate was purchased from Sigma-Aldrich (St. Louis, USA). The 0.2 μm-Nylon syringe filter was purchased from Filtep-Bio (Nantong, China). A dialysis bag (1,000 Da) was purchased from CelluSep H1. Membrane filtration productions, Inc (Texas, USA). Deionised water was used in all experiments. EBI was performed on an electron beam accelerator, MB 20-16 Mevex (Canada). The zeta potentials and hydrodynamic diameter were obtained on a Malvern Panalytical Zetasizer Ultra (United Kingdom). Fourier-transformed infrared spectroscopy (FTIR) spectra were measured on Thermo Scientific Nicolet is5/iD7 ATR (MA, USA). UV-Vis absorption spectra were explored on a Perkin Elmer Lambda 35 UV/Visible spectrometer (USA). Fluorescence emission spectra were collected on Hitachi F-4600 fluorescence spectrophotometer (Japan). The X-ray photoelectron spectrum (XPS) was collected on the Kratos AXIS Ultra DLD (Shimadzu, Japan).

2.2 Synthesis of CDs

WH leaves were collected from Pathum Thani Province, Thailand. The leaves were dried in a hot-air oven at 80°C for 3 days, followed by blending to obtain the green powder. The obtained powder was irradiated with different doses of the electron beam in the range of 100 kGy–400 kGy. The EBI powder (1.0 g) dissolved in deionised water (60 ml) was sonicated for 30 min. The mixture was

transferred to a hydrothermal teflon reactor (150 ml) and then heated at 150°C, 200°C or 250°C for 3 h. The resulting mixture was filtered through filter paper (No. 1) and 0.2 μm-nylon syringe filter, respectively. The filtered solution was dialysed in deionised water through a dialysis membrane (1,000 Da) for 2 days and then freeze-dried to obtain the brown solid for further analysis.

2.3 Fluorescence QY

The QY (Φ) of CDs was investigated in deionised water, while quinine sulfate monohydrate in 0.1 M H_2SO_4 was used as a standard reference.[34] The QY was determined according to the following Equation 1:

$$\Phi_x = \Phi_{ST} \frac{Slope_x}{Slope_{ST}} \frac{\eta_x^2}{\eta_{ST}^2} \quad (1)$$

The subscripts *ST* and *X* represent the standard reference and the sample tested, respectively. Slope denotes the slope from the linear plot of the integrated fluorescence intensity and absorbance and η denotes the refractive index of the solvent.

3. RESULTS AND DISCUSSION

3.1 WH Biomass Characterisation after EBI Pretreatment

The bright green colour in WH biomass resulted from chlorophyll content and changed significantly to faded green after the EBI pretreatment, as shown in Figure 1. The nitrogen and carbon compositions of WH powder were also elucidated by CNH analysis, as presented in Table 1. The nitrogen content of WH biomass was 4.25% without pretreatment and reduced to approximately 2.05%–2.73% after the EBI dose of 100 kGy–300 kGy. The nitrogen contents of WH biomass also decreased according to the increasing EBI dose, which is the same trend as the colour fading. Notably, the nitrogen content was determined to be 3.48% after the EBI pretreatment at 400 kGy, indicating that the EBI pretreatment caused a degradation of chlorophyll and a reduction of nitrogen content.

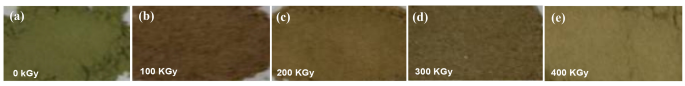

Figure 1: Optical images of WH biomass powder after EBI pretreatment at (a) 0 kGy, (b) 100 kGy, (c) 200 kGy, (d) 300 kGy and (e) 400 kGy.

Table 1: The nitrogen and carbon compositions in WH powder after EBI pretreatment.

Electron beam doses (kGy)	% N	% C
0	4.25	41.68
100	2.73	49.47
200	2.85	40.22
300	2.05	39.74
400	3.48	39.88

The effect of hydrothermal temperatures on the WH biomass morphology was also investigated by SEM, as presented in Figure 2. The plant cell wall structure was clearly observed after hydrothermal treatment at 150°C but was degraded at 200°C and 250°C. The fiber-like structure was found in the WH biomass treated with hydrothermal at 250°C, which possibly originated from the degradation of the lignocellulose structure. The hydrogen bonds were cleaved at 200°C, and the sphere structures of hydrochar were formed at 250°C since hydrochar consisted of a hydrophobic aromatic nucleus with a hydrophilic shell.[35] The rigid lignocellulose structure associated with hydrogen bonds between cellulose and hemicellulose, as well as covalent bonds with lignin, was destroyed during hydrothermal processes, leading to oligosaccharide or glucose formation.[12] Further hydrolysis, cross-linking and condensation could occur at the core of the carbonaceous material of hydrochar.[35]

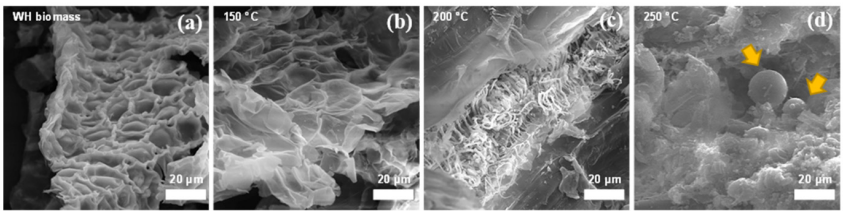

Figure 2: SEM images of (a) WH biomass powder after hydrothermal at (b) 150°C, (c) 200°C and (d) 250°C.

3.2 Characterisation of As-synthesised CDs

The effects of EBI pretreatment dosage and hydrothermal temperatures on the yield of CDs are shown in Table 2. For unirradiated WH (0 kGy), there was no difference in the CDs yields according to hydrothermal temperatures, whereas a significant difference was observed for CDs after the EBI pretreatment. At the

EBI dose of 100 kGy, the percentage yield of CDs was 13.8%, 22.0% and 10.0% at the hydrothermal temperatures of 150°C, 200°C and 250°C, respectively. Furthermore, the percentage yield of CDs synthesised via the hydrothermal method at 150°C increased from 3.8% (0 kGy) to 20.0% (400 kGy) and slightly fluctuated according to EBI pretreatment, suggesting that EBI can assist the hydrothermal conversion of LCB to CDs. For the optical properties, the QY of CDs was also investigated in deionised water, as presented in Table 2. The QY of CDs from WH with and without EBI pretreatment via hydrothermal at 150°C and 200°C was no different. However, the QY via hydrothermal at 250°C increased according to EBI doses. The maximal QY of CDs prepared from an EBI dose of 400 kGy and hydrothermal at 250°C was found to be 14.5%, suggesting that EBI pretreatment improves the optical properties of CDs. In addition, the hydrothermal temperature of 250°C was reported that cellulose and hemicellulose were hydrolysed to oligomers and glucose, which eased further polymerisation into CDs. Therefore, the combination of 400 kGy-EBI pretreatment and 250°C-hydrothermal provided the highest %QY and %yield of the CDs.

Table 2: Product yield (% yield) and % QY of CDs derived from WH biomass.

Electron beam dose (kGy)	Hydrothermal temperature					
	150°C		200°C		250°C	
	% yield	% QY	% yield	% QY	% yield	% QY
0	3.8	1.0	4.0	0.9	3.8	4.0
100	13.8	1.1	22.0	1.3	10.0	2.8
200	17.5	0.8	10.0	1.4	2.5	3.7
300	13.8	0.9	22.5	1.0	9.2	4.4
400	20.0	1.0	13.0	1.1	7.5	14.7

The hydrodynamic diameter and zeta potential of CDs (1.0 mg/ml) in deionised water were studied by the dynamic light scattering (DLS) method, as shown in Figure 3. All synthesised CDs exhibited negative zeta potentials in the range of −20.0 mV to −12.5 mV. Without EBI pretreatment, the hydrodynamic diameter of CDs increased according to hydrothermal temperatures. A similar trend was observed in the CDs with EBI pretreatment at 100 kGy. These results agree with the previous reports, where the particle sizes of lignocellulose-based CDs increased with increasing hydrothermal temperatures and the time used for the synthesis.[36] For EBI pretreatment at 300 kGy–400 kGy, the hydrodynamic diameter of CDs decreased significantly at the hydrothermal temperature of 250°C.

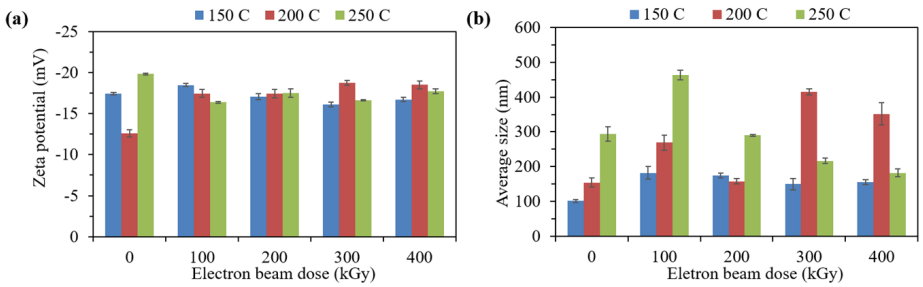

Figure 3: (a) Zeta potentials and (b) average sizes of CDs from WH via hydrothermal at 150°C–250°C with and without EBI pretreatment (100 kGy–400 kGy).

The effect of hydrothermal temperatures on the chemical properties of as-synthesised CDs without EBI pretreatment was investigated, as shown in Figure 4(a). The O-H stretching intensities (3,288 cm^{-1}) decreased at hydrothermal temperatures of 200°C and 250°C. The C-O stretching of alcohol at 1,050 cm^{-1} also decreased significantly at 200°C and 250°C. The C-H stretching of all CDs showed at 2,975 cm^{-1}. However, the peak at 1,767 cm^{-1} (C=O stretching of carboxylic acid) disappeared at 200°C and 250°C. For the C=C stretching, the peak at 1,650 cm^{-1} decreases significantly at 200°C. Notably, the peaks at 1,684 cm^{-1} and 1,598 cm^{-1} were found at 250°C, attributed to the C=O stretching of aldehydes and the C=C stretching of aromatic compounds, respectively. During hydrothermal processes, lignocellulose was depolymerised to produce monomers from decomposition reactions such as cleavage, dehydration and decarboxylation.[37] A high range of ionisation constants indicates that a large amount of H^+ and OH^- ions activated the hydrolysis process of lignocellulose and functional groups such as OH and COOH, which were cleaved to become small molecules and miscible with water.[17] Sugar units such as glucose derived from lignocellulose breakdown can be converted to 5-hydroxymethylfurfural (HMF) and dehydrated further into aromatic carbonaceous structures to create the carbon skeletons of CDs.[17]

The effect of EBI pretreatment on the surface chemistry of CDs via hydrothermal at 250°C was also investigated, as presented in Figure 4(b). Almost all of the EBI-pretreated CDs contained similar functional groups as CDs without EBI pretreatment. In the EBI pretreatment at 400 kGy, the CDs exhibited a low intensity of O-H stretching (3,288 cm^{-1}) and had a strong peak at 1,150 cm^{-1}, which was attributed to the C-O stretching of ether or ester.

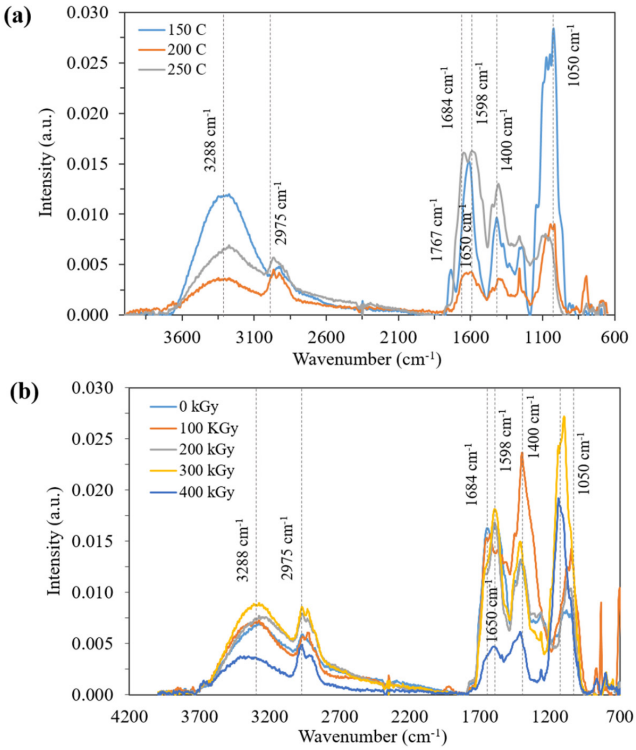

Figure 4: FTIR spectra of CDs synthesised via (a) hydrothermal method at 150°C, 200°C and 250°C and (b) hydrothermal method at 250°C with EBI pretreatment at 100 kGy, 200 kGy, 300 kGy and 400 kGy.

The chemical composition was further investigated by the XPS technique, as shown in Figure 5. The WH-derived CDs via hydrothermal at 250°C with EBI pretreatment at 400 kGy consisted of C1s (285 eV, 43.20%), O1s (532 eV, 31.03%), N1s (400 eV, 2.25%) and S2p (169 eV, 5.93%), as illustrated in Figure 5(a). The devolution C1s peak exhibited five components: C-C (284.2 eV), C=C (285.2 eV), C-O (286.1 eV), C=O (287.4 eV) and O-C=O (289.8 eV). The N1s devolution peaks comprised pyridine-N (399.7 eV) and pyrrolic-N (401.1 eV). A small amount of S2p was found, which included SO_4^{2-} (163.7 eV) and C-SO_2 (165.2 eV). The O1s devolution peaks corresponded to C1s, which consisted of C-O (531.5 eV), C=O (532.4 eV), O-H (533.9 eV) and H_2O (534.5 eV). Nitrogen and sulfur are natural minerals found in WH. The XPS results agrees with the FTIR results.

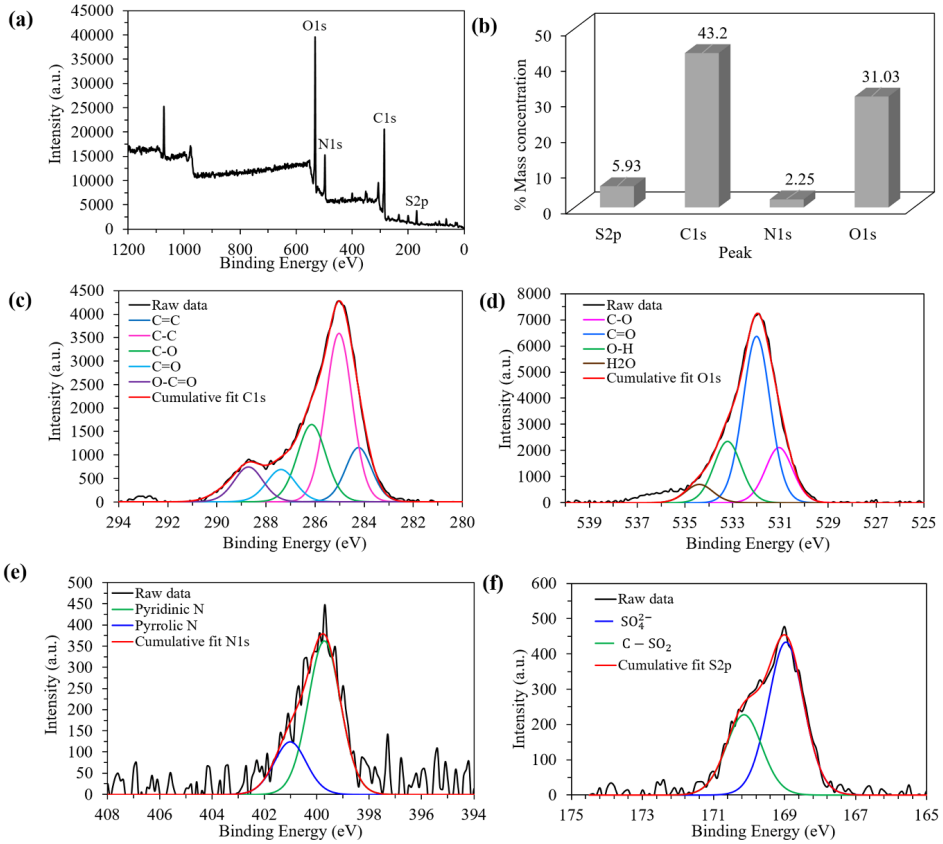

Figure 5: (a) Survey spectrum, (b) graph of % mass concentration and high-resolution spectra of (c) C1s, (d) O1s, (e) N1s and (f) S2p of CDs from WH via hydrothermal at 250°C with EBI at 400 kGy.

Two optical absorption bands at approximately 285 nm and 325 nm were observed, corresponding to the $\pi \rightarrow \pi^*$ transition of S2p carbons and the $n \rightarrow \pi^*$ transition of C=O bonds in the structure of the CDs, respectively.[38] Figure 6 shows no difference in the absorption peaks of CDs synthesised at the same hydrothermal temperature with or without EBI pretreatment. The maximum absorption wavelength of the CDs synthesised at 250°C with the EBI pretreatment at 400 kGy exhibited a slight red-shift compared to the other doses tested.

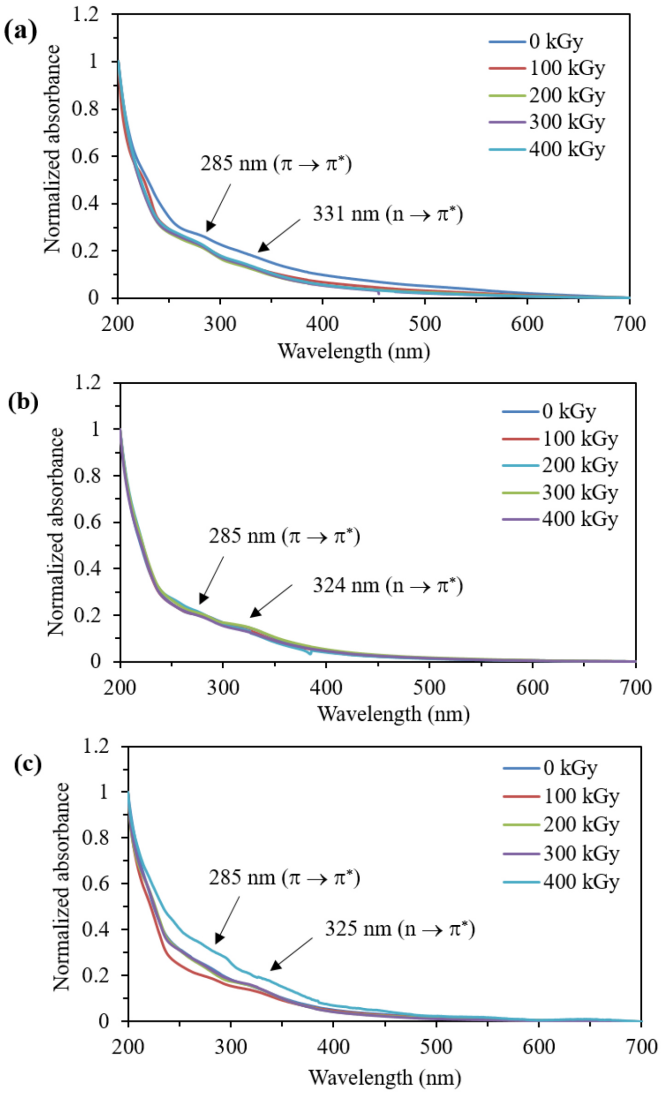

Figure 6: UV-Vis absorption spectra of CDs from WH via hydrothermal at (a) 150°C, (b) 200°C and (c) 250°C with EBI pretreatment at 0 kGy, 100 kGy, 200 kGy, 300 kGy and 400 kGy.

The fluorescence emission spectra of CDs were also studied in deionised water at excitation wavelengths of 240 nm–500 nm, as shown in Figure 7. The fluorescence emission spectra of all as-synthesised CDs with or without EBI pretreatment displayed tunable fluorescence emission with different excitation wavelengths. The fluorescence emission spectra of CDs synthesised at 150°C–250°C without

EBI pretreatment showed a blue shift of the maximum emission wavelength (λ_{em}) from 150°C to 250°C. For EBI pretreatment, λ_{em} of the as synthesised-CDs at 150°C exhibited a blue shift when the excitation at the UV region, whereas the excitation in the visible region showed λ_{em} in the range of 551 nm–563 nm. With the increasing EBI dose, λ_{em} in the visible region slightly decreased. Interestingly, the CDs synthesised at 200°C and 250°C showed an increase λ_{em} with the EBI dose. However, the higher doses of EBI, the lower λ_{em} in the UV region and the greater λ_{em} in the visible region.

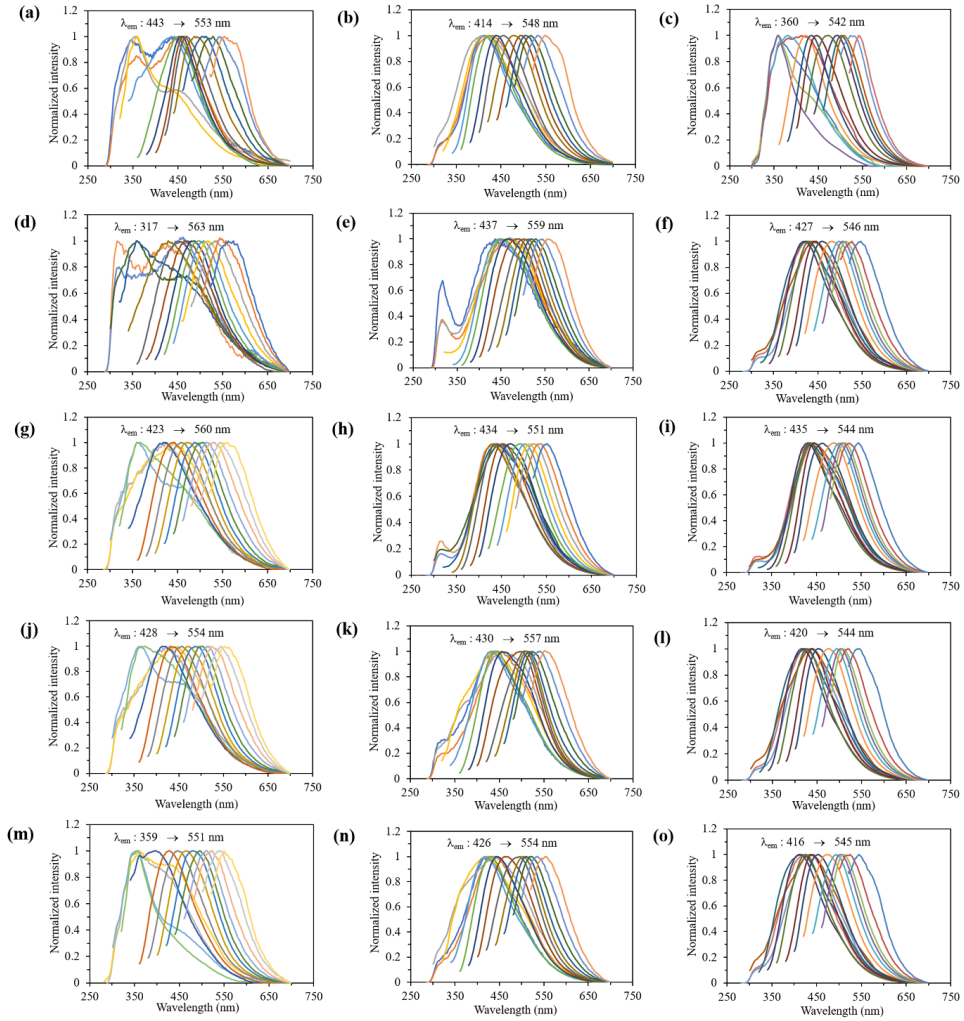

Figure 7: Fluorescence emission spectra of CDs synthesised via hydrothermal method at (a, d, g, j, m) 150°C, (b, e, h, k, n) 200°C and (c, f, i, l, o) 250°C with EBI pretreatment at (d–f) 100 kGy, (g–i) 200 kGy, (j–l) 300 kGy and (m–o) 400 kGy.

In addition, the photostability and photobleaching of CDs with the EBI pretreatment of 400 kGy synthesised via hydrothermal at 250°C were also studied in deionised water (Figure 8). The CDs exhibited higher than 90% of the relative fluorescence intensity (F/F_0) under UV illumination at 365 nm for 60 min, indicating that the CDs did not show photobleaching. The fluorescence emission of the CDs also showed no change under visible light at room temperature, suggesting that the CDs had a high photostability property. Furthermore, the effects of pH buffer and high salt medium of CDs with the EBI pretreatment of 400 kGy synthesised via hydrothermal at 250°C were investigated for fluorescence emission. Figure 8(c) shows that the relative fluorescence intensity of CDs was higher in weak acidic (pH 5) and neutral (pH 7) than in basic conditions (pH 9–11). The CDs exhibited 97% of the relative fluorescence intensity in the presence of NaCl (2.0 M), indicating that high salt concentrations did not affect the fluorescence emission of the CDs. These results indicated that CDs could potentially be applied in several potential applications, such as bio-imaging or fluorescence sensors.

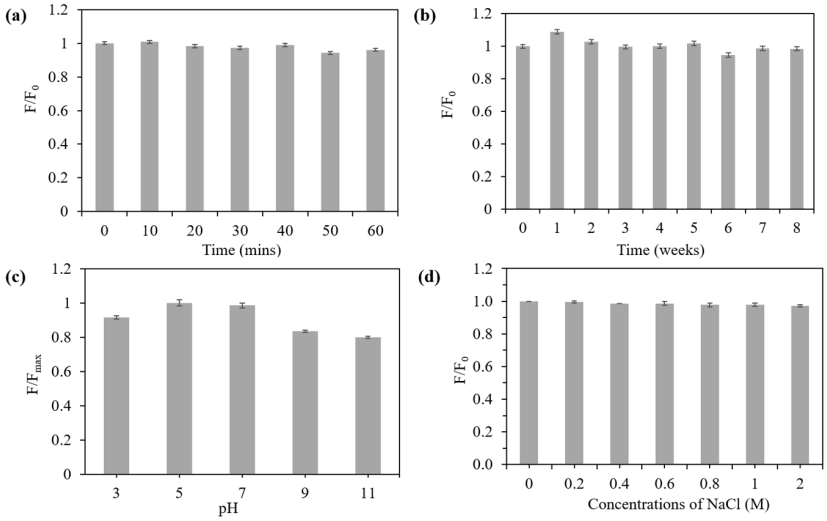

Figure 8: The relative fluorescence intensity of CDs (1.0 mg/ml) with EBI pretreatment of 400 kGy synthesised via hydrothermal at 250°C (a) under UV irradiation at 365 nm, (b) under visible light at room temperature, (c) in the buffer solution at different pH and (d) in the presence of NaCl (0 M–2 M).

4. CONCLUSION

This research showed that EBI pretreatment at 400 kGy can assist in the hydrothermal conversion (250°C) of WH biomass to CDs. The method resulted in a higher product yield (7.5%) and better fluorescence properties (QY of 14.5%). At hydrothermal temperatures of 150°C and 250°C, the QY of as-synthesised CDs was only 1.0%–1.5%. The hydrothermal temperatures affected the particle sizes and surface chemistry of the CDs. The EBI pretreatment induced the degradation of the lignocellulose structure in WH and facilitated the depolymerisation of hydrothermal conversion. Furthermore, the CDs with higher doses of EBI pretreatment displayed a lower emission wavelength in the UV region and a greater emission wavelength in the visible region. The as-synthesised CDs exhibited high photostability and no photobleaching. The effect of the high salt concentration showed no influence on the fluorescence emission of the CDs.

5. ACKNOWLEDGEMENTS

This work was supported by Thailand Institute of Nuclear Technology (TINT), Thailand Science Research and Innovation (TSRI), and National Science, Research and Innovation Fund (NSRF). We would like to thank RMUTT Central Lab, Institute of Research and Development, Rajamangala University of Technology Thanyaburi, for facility support.

6. REFERENCES

1. Gaurav, G. K. et al. (2020). Water hyacinth as a biomass: A review. *J. Clean. Prod.*, 277, 122214. https://doi.org/10.1016/j.jclepro.2020.122214
2. Narayanan, M. et al. (2021). Water hyacinth biochar and Aspergillus niger biomass amalgamation potential in removal of pollutants from polluted lake water. *J. Environ. Chem. Eng.*, 9(4), 105574. https://doi.org/10.1016/j.jece.2021.105574
3. Li, F. et al. (2021). Water hyacinth for energy and environmental applications: A review. *Bioresour. Technol.*, 327, 124809. https://doi.org/10.1016/j.biortech.2021.124809
4. Merry M. & Mitan, N. (2019). Water hyacinth: Potential and Threat. *Mater. Today: Proc.*, 19, 1408–1412. https://doi.org/10.1016/j.matpr.2019.11.160
5. Merklein, K. et al. (2016). Chapter 11 - Biomass Utilization. In Eckert, C. A. & Trinh, C. T. (Eds.). *Biotechnology for Biofuel Production and Optimization*. Elsevier: Amsterdam, 291–324. https://doi.org/10.1016/B978-0-444-63475-7.00011-X
6. Isikgor, F. H. & Becer, C. R. (2015). Lignocellulosic biomass: A sustainable platform for the production of bio-based chemicals and polymers. *Polym. Chem.*, 6(25), 4497–4559. https://doi.org/10.1039/C5PY00263J

7. Kumar, B. et al. (2020). Current perspective on pretreatment technologies using lignocellulosic biomass: An emerging biorefinery concept. *Fuel Process. Technol.*, 199. https://doi.org/10.1016/j.fuproc.2019.106244
8. Yoo, J. et al. (2011). Thermo-mechanical extrusion pretreatment for conversion of soybean hulls to fermentable sugars. *Bioresour. Technol.*, 102(16), 7583–7590. https://doi.org/10.1016/j.biortech.2011.04.092
9. Liu, Q. et al. (2016). Pretreatment of corn stover for sugar production using a two-stage dilute acid followed by wet-milling pretreatment process. *Bioresour. Technol.*, 211, 435–442. https://doi.org/10.1016/j.biortech.2016.03.131
10. Shahabazuddin, M. et al. (2018). Thermal assisted alkaline pretreatment of rice husk for enhanced biomass deconstruction and enzymatic saccharification: Physico-chemical and structural characterization. *Bioresour. Technol.*, 263, 199–206. https://doi.org/10.1016/j.biortech.2018.04.027
11. Sheikh, M. M. I. et al. (2015). A synergistic effect of pretreatment on cell wall structural changes in barley straw (*Hordeum vulgare L.*) for efficient bioethanol production. *J. Sci. Food Agric.*, 95(4), 843–850. https://doi.org/10.1002/jsfa.7004
12. Al-Assaf, S. et al. (2016). *The Radiation Chemistry of Polysaccharides*. International Atomic Energy Agency: Vienna.
13. Hyun Hong, S. et al. (2014). Improved enzymatic hydrolysis of wheat straw by combined use of gamma ray and dilute acid for bioethanol production. *Radiat. Phys. Chem.*, 94, 231–235. https://doi.org/10.1016/j.radphyschem.2013.05.056
14. Swallow, A. J. & Charlesby, A. (2016). *Radiation Chemistry of Organic Compounds: International Series of Monographs on Radiation Effects in Materials*. Elsevier Science.
15. Abbas, A. et al. (2018). Biomass-waste derived graphene quantum dots and their applications. *Carbon*, 140, 77–99. https://doi.org/10.1016/j.carbon.2018.08.016
16. Den, W. et al. (2018). Lignocellulosic biomass transformations via greener oxidative pretreatment processes: Access to energy and value-added chemicals. *Front. Chem.*, 6, 141. https://doi.org/10.3389/fchem.2018.00141
17. Khan, T. A. et al. (2019). Hydrothermal carbonization of lignocellulosic biomass for carbon rich material preparation: A review. *Biomass Bioenergy*, 130, 105384. https://doi.org/10.1016/j.biombioe.2019.105384
18. Qi, H. et al. (2019). Biomass-derived nitrogen-doped carbon quantum dots: Highly selective fluorescent probe for detecting Fe^{3+} ions and tetracyclines. *J. Colloid Interface Sci.*, 539, 332–341. https://doi.org/10.1016/j.jcis.2018.12.047
19. Karahan, H. E. et al. (2020). Biomass-derived nanocarbon materials for biological applications: Challenges and prospects. *J. Mater. Chem. B*, 8(42), 9668–9678. https://doi.org/10.1039/D0TB01027H
20. Tejwan, N. et al. (2020). Multifaceted applications of green carbon dots synthesized from renewable sources. *Adv. Colloid Interface Sci.*, 275, 102046. https://doi.org/10.1016/j.cis.2019.102046
21. Semeniuk, M. et al. (2019). Future perspectives and review on organic carbon dots in electronic applications. *ACS Nano*, 13(6), 6224–6255. https://doi.org/10.1021/acsnano.9b00688

22. Atchudan, R. et al. (2022). Tunable fluorescent carbon dots from biowaste as fluorescence ink and imaging human normal and cancer cells. *Environ. Res.*, 204, 112365. https://doi.org/10.1016/j.envres.2021.112365
23. Jelinek, R. (2016). *Carbon quantum dots.* Springer International Publishing. https://doi.org/10.1007/978-3-319-43911-2
24. Yang, S. et al. (2014). Large-scale fabrication of heavy doped carbon quantum dots with tunable-photoluminescence and sensitive fluorescence detection. *J. Mater. Chem. A*, 2(23), 8660–8667. https://doi.org/10.1039/C4TA00860J
25. Suryawanshi, A. et al. (2014). Large scale synthesis of graphene quantum dots (GQDs) from waste biomass and their use as an efficient and selective photoluminescence on–off–on probe for Ag^{+} ions. *Nanoscale*, 6(20), 11664–11670. https://doi.org/10.1039/C4NR02494J
26. Pan, D. et al. (2010). Hydrothermal route for cutting graphene sheets into blue-luminescent graphene quantum dots. *Adv. Mater.*, 22(6), 734–738. https://doi.org/10.1002/adma.200902825
27. Atchudan, R. et al. (2017). Facile green synthesis of nitrogen-doped carbon dots using Chionanthus retusus fruit extract and investigation of their suitability for metal ion sensing and biological applications. *Sens. Actuators B Chem.*, 246, 497–509. https://doi.org/10.1016/j.snb.2017.02.119
28. Liu, M. L. et al. (2019). Carbon dots: Synthesis, formation mechanism, fluorescence origin and sensing applications. *Green Chem.*, 21 (3), 449–471. https://doi.org/10.1039/C8GC02736F
29. Jelinek, R. (2016) *Carbon Quantum Dots: Synthesis, Properties and Applications*. Springer International Publishing.
30. Krishnaiah, P. et al. (2022). Utilization of waste biomass of Poa pratensis for green synthesis of n-doped carbon dots and its application in detection of Mn^{2+} and Fe^{3+}. *Chemosphere*, 286, 131764. https://doi.org/10.1016/j.chemosphere.2021.131764
31. Atchudan, R. et al. (2018). Highly fluorescent nitrogen-doped carbon dots derived from Phyllanthus acidus utilized as a fluorescent probe for label-free selective detection of Fe^{3+} ions, live cell imaging and fluorescent ink. *Biosensors Bioelectron.*, 99, 303–311. https://doi.org/10.1016/j.bios.2017.07.076
32. Atchudan, R. et al. (2020). Hydrophilic nitrogen-doped carbon dots from biowaste using dwarf banana peel for environmental and biological applications. *Fuel*, 275, 117821. https://doi.org/10.1016/j.fuel.2020.117821
33. Roy, P. et al. (2014). Plant leaf-derived graphene quantum dots and applications for white LEDs. *New J. Chem.*, 38 (10), 4946–4951. https://doi.org/10.1039/C4NJ01185F
34. Wechakorn, K. et al. (2020). Synthesis of carbon quantum dot from water hyacinth stalk by radiation processing. *Orient. J. Chem.*, 36, 897–902. https://doi.org/10.13005/ojc/360514
35. Wang, T. et al. (2018). A review of the hydrothermal carbonization of biomass waste for hydrochar formation: Process conditions, fundamentals, and physicochemical. *Renewable Sustainable Energy Rev.*, 90, 223–247. https://doi.org/10.1016/j.rser.2018.03.071

36. Zhang, J. et al. (2022). Co-production of carbon quantum dots and biofuels via hydrothermal conversion of biomass. *Fuel Process. Technol.*, 232, 107276. https://doi.org/10.1016/j.fuproc.2022.107276
37. Xu, Y. H. & Li, M. F. (2021). Hydrothermal liquefaction of lignocellulose for value-added products: Mechanism, parameter and production application. *Bioresour. Technol.*, 342, 126035. https://doi.org/10.1016/j.biortech.2021.126035
38. Kwamman, T. et al. (2021). Poly(vinyl)alcohol film composited with carbon dots from water hyacinth stalks based on gamma irradiation for the UV blocking film. *J. Met. Mater. Miner.*, 31(4), 123–128. https://doi.org/10.14456/jmmm.2021.67